

## Full Length Article

Effects of O<sub>2</sub> concentration of O<sub>2</sub>/CO<sub>2</sub> co-flow on the flame stability of non-premixed coaxial jet flame

Taesung Kim\*, Muhammad Bukar, Suman Basnet, Gaetano Magnotti

Clean Combustion Research Center (CCRC), King Abdullah University of Science and Technology (KAUST), Thuwal 23955-6900, Saudi Arabia

## ARTICLE INFO

**Keywords:**  
 Methane O<sub>2</sub>-CO<sub>2</sub> flame  
 Liftoff condition  
 Flame stability  
 Effective velocity  
 Turbulent flame speed

## ABSTRACT

Greenhouse gas emissions should be reduced to stop the advance of global warming. Oxy-fuel combustion is one of the methods to reduce CO<sub>2</sub> emissions. This paper aims to study the stabilization of CO<sub>2</sub>-diluted oxy-methane non-premixed jet flames and compare this with the results of methane-air flames. The lower the co-flow velocity and the higher the oxygen concentration in the co-flow, the higher the stability. If the flame stability is strong enough to withstand flame shape changes from the over-ventilated flame to the under-ventilated flame, the flammable range without blowout increases significantly under the under-ventilated flame. Otherwise, by decreasing the liftoff flame stability, the over-ventilated flame cannot change to the under-ventilated flame and blows out near the globally stoichiometric condition. The flame stability of a CO<sub>2</sub>-diluted oxy-fuel flame can differ from that of methane-air flames due to the properties of CO<sub>2</sub> and N<sub>2</sub>. The effective velocity proposed by Guiberti et al. shows a good collapse of the dimensionless liftoff height among the O<sub>2</sub>/CO<sub>2</sub> co-flow, but the dimensionless liftoff height under the air co-flow is not on the same line with the O<sub>2</sub>/CO<sub>2</sub> co-flow. This study suggests a modified dimensionless liftoff height equation considering the fuel and co-flow mixture kinematic viscosity instead of the fuel kinematic viscosity and the ratio of the thermal diffusivity of the mixture. The thermal diffusivity ratio does not affect the result of the air co-flow. Additionally, the new coefficient  $\beta$  and turbulent Schmidt number are suggested because these numbers are factors depending on the burner geometry. The modified effective velocity using new coefficients and the modified dimensionless liftoff height show a good collapse for not only O<sub>2</sub>/CO<sub>2</sub> co-flows but also air co-flow. Also, the modified effective velocity shows the possibility of the critical liftoff velocity prediction.

## 1. Introduction

Greenhouse gas emissions should be reduced to stop the advance of global warming. Government and electricity providers focus on renewable energy, such as solar, wind, and hydropower. Nonetheless, the energy from combustion will be one of the primary electricity sources over the following decades. To fulfill the reduction target of greenhouse emissions, however, the concept of combustion should be changed.

Oxy-fuel combustion is one of the methods to reduce CO<sub>2</sub> emissions. The product of oxy-combustion is carbon dioxide and water vapor with hydrocarbon fuels. So, CO<sub>2</sub> emission can be reduced significantly by combining carbon capture and storage [1,2] or supercritical CO<sub>2</sub> cycle [3]. Furthermore, oxy-combustion can remove NOx emission if the fuel does not include the nitrogen molecule.

However, it is challenging to use oxy-fuel combustion for the

industrial field due to too high flame temperature. Dilution of other gases is needed to reduce the flame temperature. Regarding the primary purpose of oxy-fuel combustion, additional CO<sub>2</sub> gas can be a good dilution gas.

The flame stability of oxy-fuel flame can differ from fuel-air flames due to differences in properties between CO<sub>2</sub> and N<sub>2</sub>. For example, the laminar flame speed decreases faster with CO<sub>2</sub> dilution. This study aims to describe the stabilization of CO<sub>2</sub> diluted non-premixed jet methane oxy-flames and compare this with the result of methane-air flames. Considering the heat capacity difference between CO<sub>2</sub> and N<sub>2</sub>, the CO<sub>2</sub> concentration of oxidizer gas is adjusted to keep the same adiabatic flame temperature.

In terms of the premixed flame, averaged flame length and fuel consumption speed decrease. The flame surface density (average flame area per unit volume) increases when N<sub>2</sub> of air is substituted to CO<sub>2</sub> as keeping constant equivalence ratio and Reynolds number [4]. CO<sub>2</sub>

\* Corresponding author at: Physical Science and Engineering Division, King Abdullah University of Science and Technology (KAUST), Thuwal 23955-6900, Saudi Arabia.

E-mail address: [taesung.kim@kaust.edu.sa](mailto:taesung.kim@kaust.edu.sa) (T. Kim).

## Nomenclature

$S_L$	Laminar flame speed [m/s]
$\rho$	Density [kg/m <sup>3</sup> ]
$\mu$	Dynamic viscosity [kg/ms]
$\nu$	Kinematic viscosity [m <sup>2</sup> /s]
$Z_{st}$	Stoichiometric mixture fraction
$\alpha$	Thermal diffusivity [m <sup>2</sup> /s]
$Sc_t$	Turbulent Schmidt number
$h$	Liftoff height [mm]
Subscript f	Fuel
Subscript co	Co-flow
Subscript mix	Fuel-oxidizer mixture
Subscript eff	Effective

diluted flames are also less stable near blowoff conditions. But, the velocity distribution of both N<sub>2</sub> and CO<sub>2</sub> diluted flames is very similar [5]. The effects of CO<sub>2</sub> dilution on the flammable limit, flame propagating velocity, and quenching distance are larger than that of N<sub>2</sub> dilution. CO<sub>2</sub> diluted flames have a narrower flammable range than N<sub>2</sub> diluted flames. The flame speed decreases significantly. The effects of CO<sub>2</sub> on the flame propagating velocity and laminar burning velocity are the maximum near the stoichiometric condition [6,7].

Similar to the premixed flame, the flammability and the flame stability also decrease with CO<sub>2</sub> dilution at the diffusion flames. The dilution mole fraction of the flame extinction decreases due to the chemical effects of CO<sub>2</sub> [8]. At the coaxial diffusion jet flame, the liftoff coaxial-flow velocity decreases when the N<sub>2</sub> is replaced by the CO<sub>2</sub> [9]. With the confined burner, the wall temperature can affect the flame length and the liftoff height [10].

CO<sub>2</sub> dilution occurs a larger laminar flame speed decreases due to the heat capacity increases, low thermal diffusivity, and CO<sub>2</sub> dissociation. Considering the reaction pathway, CO<sub>2</sub> makes slow flame speed because combustion reactants, intermediate, and product concentration decreases, although the major pathway of CH<sub>4</sub> oxidation does not change due to CO<sub>2</sub> dilution. The effect of CO<sub>2</sub> dissociation is less critical with high CO<sub>2</sub> dilution because the flame temperature is affected significantly in this case [11–13]. The lower flammable limit also increases with CO<sub>2</sub> dilution in the same concentration of oxygen due to the chemical effect of CO<sub>2</sub> [14]. In previous diffusion flame studies, the adiabatic flame temperature and the laminar flame speed have not been considered to compare the flame stability with air conditions. So, in this study, the various O<sub>2</sub>/CO<sub>2</sub> ratios are considered to have the same adiabatic flame temperature (O<sub>2</sub>/CO<sub>2</sub> = 32/68, T<sub>ad, air</sub> = 2225 K, T<sub>ad, 32/68</sub> = 2220 K) and a similar laminar flame speed (O<sub>2</sub>/CO<sub>2</sub> = 40/60, S<sub>L,air</sub> = 0.39 m/s, S<sub>L, 40/60</sub> = 0.43 m/s).

In terms of diffusion jet flames that we focus on, the stability mechanism of lifted flames has been reported in many studies. The lifted flames have a tri-branched structure at the flame base to stabilize. Tri-branched flames include rich and lean premixed flames and diffusion flames at the flame base. So, there is an almost stoichiometric premixed flame near the flame base. And then, the flow velocity at the flame base can decrease due to diverge the streamline near this triple point [15,16]. Triple flames are also important not only for the liftoff but also for the blowoff phenomena. The stoichiometric contour line of flames based on the flow conditions plays a role in the blowoff [17]. The co-flow velocity also affects the blowoff limit of lifted flames. The blowoff limit of lifted flames increases linearly until reaching the peak initially. After that, the blowoff limit decreases very fast as increasing co-flow velocity [18].

The major lifting criteria for diffusion jet flames depend on flow conditions, fuel types, and the burner geometry [19]. Lifted flames are stabilized in a turbulent region. The flame can be stabilized when the gas flow velocity is balanced with the turbulent flame speed. The flame can

be blown out when the turbulent flame speed is higher than the local flow velocity [20–23]. Within certain conditions, the lifted flames are stabilized when the local gas velocity is lower than three times the laminar flame speed [16,23–25] or 25 times the laminar flame speed [26].

One of the main parameters of the liftoff flame is the liftoff height. The various simple correlations are suggested to predict the liftoff height of the non-premixed jet flame depending on the experimental results. Kalghatgi [27] suggested the dimensionless liftoff height as similar to the Reynolds number definition and showed the dimensionless liftoff height as a function of the jet velocity, the laminar burning velocity, and the density function at the jet flame without the co-flow.

$$\frac{\rho_f S_L h_f}{\mu_f} = C_1 \frac{U_j}{S_L} g(\bar{\rho}) \quad (1)$$

where  $\rho_f$  is the fuel density,  $\mu_f$  is the dynamic viscosity of the fuel,  $S_L$  is the laminar flame speed,  $h$  is the liftoff height,  $U_j$  is the jet velocity,  $C_1$  is the empirical coefficient about 50, and  $g(\bar{\rho})$  is the density function as  $g(\bar{\rho}) = 0.04 + 0.46\bar{\rho} + 0.5\bar{\rho}^2$  with  $\bar{\rho} = \rho_{fuel}/\rho_{air}$ .

Upatnieks et al. [28] showed the liftoff height relation based on Kalghatgi's suggestion as considering the characteristic chemical reaction rate.

$$h = C_2 \frac{U_j - S_L/Z_{st}}{S_L^2/\alpha} \quad (2)$$

where  $Z_{st}$  is the stoichiometric mixture fraction and  $\alpha$  is the thermal diffusivity. The characteristic chemical reaction rate is calculated as  $S_L^2/\alpha$ .

Considering the co-flow effect, Montgomery et al. [29] suggested the effective velocity that contains the co-flow parameters.

$$U_{eff} = U_j + C_3 \sqrt{\frac{\rho_{co}}{\rho_f}} U_{co} \quad (3)$$

where  $U_{eff}$  is the effective velocity,  $\rho_{co}$  is the co-flow density,  $U_{co}$  is the co-flow velocity, and  $C_3$  is the empirical coefficient. The empirical coefficient is chosen to be 40 for the CH<sub>4</sub>-air jet flame [30,31]. The square root density ratio term is related to the Kelvin-Helmholtz instability. Mixing degree from the Kelvin-Helmholtz instability increases in proportional to this density ratio term [32].

Guiberti et al. [33] presented the improved effective velocity based on Montgomery's effective velocity (Eq. (1)) and the stoichiometric contour velocity presented by Han et al. [34].

$$U_{eff} = U_j + \frac{1.5 \left( \frac{\rho_{co}}{\rho_f} \right)^{1.5} (U_{co} - \beta S_L)}{Sc_t Z_{st}} \quad (4)$$

where  $\beta$  is the coefficient and  $Sc_t$  is the turbulent Schmidt number. This effective velocity can show the linear relationship to the liftoff height at various fuels and elevated pressures if  $\beta$  and  $Sc_t$  are adjusted properly. Applying this effective velocity to Kalghatgi's model as the jet velocity, there is a good linear fit for the methane and ethane flames and the high-pressure conditions up to 7 bar.

With these short reviews, the stability limit of the CO<sub>2</sub> diluted flame is much less than that of methane-air flames due to the laminar flame speed, gas properties of CO<sub>2</sub>, and other chemical characteristics. In this study, the stability of CO<sub>2</sub> diluted oxy-methane flames is compared with that of methane-air flames by considering the same adiabatic flame temperature and the similar laminar flame speed. And then, following the mechanism of lifted flames, local velocity distribution describes differences between two flames and the reason for these differences. The liftoff height model of the fuel-air flame is applied to the CO<sub>2</sub> diluted oxy-methane flame and modified to fit this flame.

## 2. Experimental method

The burner is designed to investigate coaxial diffusion jet flames, as shown in Fig. 1. There are two enclosed square tubes. One is for the oxidizer co-flow stream, and the other is for the dilution gas. These square tubes can remove optical distortions and reduce the cost of high-quality optical windows rather than circular tubes.

Gaseous fuel is supplied through a stainless steel tube of 1.753 mm inner and 3.175 mm outer diameter. Co-flow oxidizer is delivered through the inner square tube with 25 mm × 25 mm of cross-sectional area and 150 mm of height. Dilution gas flows between the outer (40 mm × 40 mm cross-section and 200 mm height) and inner square tubes. The main purpose of dilution gas is to cool the burner and dilute the combustion product gas with pure CO<sub>2</sub>, such as a practical burner for the SCO<sub>2</sub> power cycle. The enclosed side walls are 2 mm thick UV fused silica windows.

The experimental conditions are shown in Table 1. Pure methane is used as a gaseous fuel. The exit fuel jet velocity is controlled from 0 to 90 m/s with a 1 m/s interval. With this jet velocity and the burner geometry, the fuel Reynolds number can increase up to 9000.

Four types of oxidizer, air, 50 %/50 %, 40 %/60 %, and 32 %/68 % of the O<sub>2</sub>/CO<sub>2</sub> mixture, are considered the co-flow. 32 %/68 % of the O<sub>2</sub>/CO<sub>2</sub> mixture concentration is determined to have the same adiabatic flame temperature as the airflow. The adiabatic flame temperature and the laminar flame speed are calculated by Chemkin-Pro with the GRI 3.0 mechanism [35]. The oxidizer co-flow velocity increases up to 1.0 m/s with various intervals from 0.0125 to 0.05 m/s. The small interval is

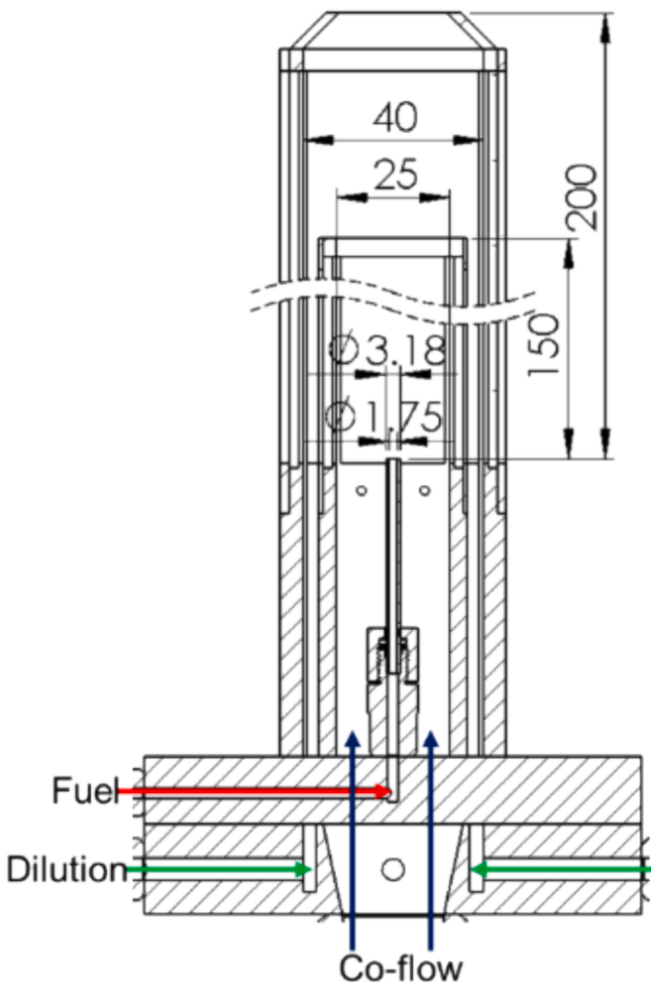


Fig. 1. Non-premixed jet flame burner enclosed inner and outer enclosures.

**Table 1**  
Experimental conditions.

Fuel type	CH <sub>4</sub>
Fuel velocity	0 to 90 m/s (1 m/s interval)
Oxidizer type	Air, O <sub>2</sub> /CO <sub>2</sub> mixture (O <sub>2</sub> /CO <sub>2</sub> = 50/50, 40/60, 32/68)
Oxidizer velocity	0 to 1 m/s (various interval from 0.0125 to 0.05 m/s)

used near the significant change point of flame stability.

Flame images are taken using a DSLR camera with two exposure times (1/100 sec for attached flames and 1 sec for liftoff flames). The accumulated flame image during an exposure time can be considered the sum of all flame images in the process of the time-averaged flame calculation. So, these images are used to show the time-averaged flame shape. The liftoff flame height is calculated by using this time-averaged flame image. Due to the turbulent, the intensity of this averaged image shows a certain distribution. So, the location of 50 % of the maximum intensity is founded, and the distance between the fuel nozzle and this location is determined as the liftoff height. This method is borrowed from a reference [33] that calculated the flame liftoff length using average OH chemiluminescence images. The criterion for the liftoff flame is the liftoff height. If the liftoff height is higher than 0.4 mm, this flame is considered the liftoff flame.

OH planar laser-induced fluorescence (PLIF) is used to measure the flame structure near the flame base point. The Nd:YAG laser (Continuum Powerlite DLS9010) pumps a dye laser (Continuum ND6000) at a 10 Hz repetition rate. After the frequency doubler at the dye laser, the output energy is 7 mJ/pulse, and the wavelength is 283.927 nm. The cylindrical lens and spherical lens are used to make the laser sheet. The intensified CCD camera (Princeton instruments PI-MAX 3) and 100 mm focal length UV lens collect the OH fluorescence signal with a 309 ± 10 nm bandpass filter.

To evaluate the hypothesis that is the relation between the turbulent flame speed and the flow velocity, we calculate the turbulent flame speed by the Eq. (5) suggested by Tieszen [21].

$$S_t = S_L + 0.64S_L^{0.5}u^{0.5} \left( \frac{uL_t}{\nu} \right)^{0.25} \quad (5)$$

$$L_t = 0.039z \left( 1 + 5.73 \left( \frac{r}{z} \right) \right) \quad (6)$$

where  $S_t$  is the turbulent flame speed,  $S_L$  is the laminar flame speed,  $u$  is the axial velocity perturbation,  $L_t$  is the turbulent integral length scale,  $\nu$  is the kinematic viscosity,  $r$  is the radial distance measured from the jet centerline, and  $z$  is the radial distance measured from the jet centerline. The turbulent integral length scale is calculated by Eq. (6) taken from Ref. 18. The calculated turbulent flame speed is well-matched with the axial velocity at liftoff height [22,27].

## 3. Data and discussion

### 3.1. Flame stability

The flame stabilization characteristics can be explained by five types. First, if the flame is anchored at the fuel nozzle tip, it is called the attached flame. Next, the liftoff flame means that the flame is detached from the fuel nozzle, increasing the fuel velocity but stabilizing somewhere. When the flame is extinguished at the higher fuel velocity after the flame is lifted off, this phenomenon is called the blowout. Or, the liftoff flame can be reattached as the fuel velocity decreases. That is called the reattached flame. Usually, the reattachment occurs at a jet velocity much lower than the liftoff jet velocity. On the contrary, blowoff means that the attached flame is blown off directly without liftoff.

As many researchers have shown, flame stabilization is governed by the fuel and co-flow velocities at the fixed burner geometry [17–26].

These can be used to characterize the flame stabilization condition. The flame stability map shown in Fig. 2 can be separated into four regions depending on the co-flow velocity in this study. One of the flame lift-off mechanisms is based on the balance between entrained velocity and the local laminar burning velocity, considering the jet and the oxidizer mixture [16]. Considering this, the higher O<sub>2</sub> concentration in the oxidizer can enhance the laminar burning velocity significantly. It can help keep the flame stable, so the flame lifts off at higher jet velocities under higher O<sub>2</sub> concentrations (Fig. 2a).

In the first region, the flame blows off directly at the low co-flow velocity. And then, the flame lifts off and blows out at the high fuel velocity in the second region. In the cases of 50%/50% and 40%/60% of the O<sub>2</sub>/CO<sub>2</sub> mixture co-flow, the blowoff phenomenon does not happen until 90 m/s of the fuel velocity, which is the limitation of the mass flow control system as shown in Fig. 2b. Although it is not possible to measure the blowoff conditions above 90 m/s of jet velocities, arbitrary lines for these two mixture concentrations are drawn to avoid confusion by indicating that blowoff does not occur at higher co-flow velocities. These arbitrary lines are to inform that the blowoff can occur at jet velocities above 90 m/s.

In the third region, the blowoff phenomenon occurs instead of the lift-off, and blowoff conditions are on one line with lift-off conditions. In this region, a little different behavior is observed according to co-flow types. The flame with the air co-flow blows off directly or lifts off and blows out at the same flow condition. As increasing the co-flow velocity, the lift-off and blowout phenomena happen again, not the blowoff, and the flame stability returns to the second region. The flame with 32%/68% of the O<sub>2</sub>/CO<sub>2</sub> mixture blows off or lifts off randomly at the low co-flow velocity in the third region. As increasing the co-flow velocity, lift-off does not occur, but the only blowoff happens. At the fourth region, the flame stability is similar to that of the second region, but blowoff fuel velocity increases as the co-flow velocity increases.

Assuming the blowoff fuel velocity in the third region as the lift-off fuel velocity, the lift-off fuel velocities of the air and O<sub>2</sub>/CO<sub>2</sub> mixture co-flows are on the one line and well-matched each other. The blowout at the third region can be initiated similarly to the lift-off. After the flame lifts off, if the flame cannot be stabled inside the burner, the flame blows off and belongs to the third region. So, lift-off flame stability can determine whether the flame lifts off or blows out from the second to the fourth region.

At the low co-flow velocity, the lifted flame stability becomes weaker as the co-flow velocity increases. So, the flame can blow out directly without the lift-off. There is the transient flame behavior between the second and the third region. In contrast, the lifted flame stability increases with the co-flow velocity increase at the relatively higher co-flow velocity. It can be confirmed that the flame lifts off instead of the blowout, and the blowoff fuel velocity increases with the higher co-flow velocity at the fourth region.

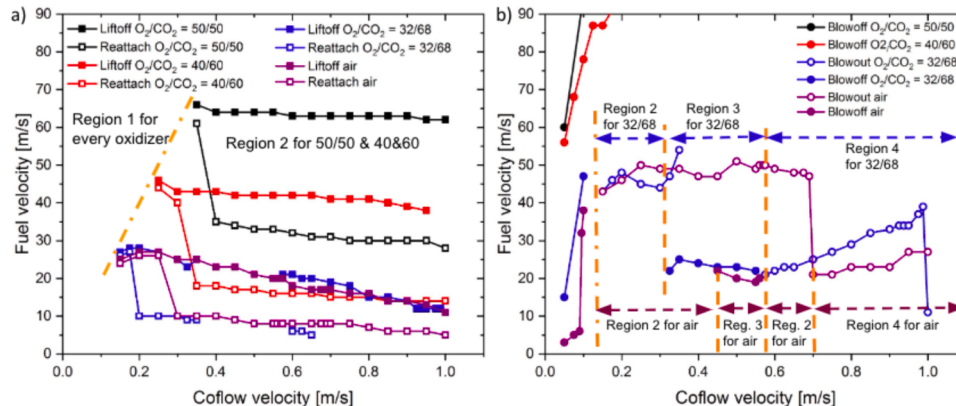


**Fig. 2.** Flame stability map, (a) liftoff and reattachment conditions and (b) blowoff and blowout conditions.

Fig. 3 shows the DSLR images of attached flames with various flow conditions. There is the center red flame at the low fuel velocity. As increasing the fuel velocity, the center red flame is disappeared because the mixing between the fuel and co-flow is enhanced. An increase in the Reynolds number of the outer flow or the outer to inner density ratio decreases the mixing degree [36]. With higher CO<sub>2</sub> concentration in the co-flow, the density increases, and the Reynolds number also increases because the kinematic viscosity decreases. But, the Reynolds number increase due to the co-flow velocity in the same O<sub>2</sub>/CO<sub>2</sub> concentration does not significantly affect the red center zone.

The shape of the lift-off flame is different according to the flame region in Fig. 2. Figs. 4–6 show DSLR averaged lift-off flame images with 1 s exposure time. At the second region, the lift-off flame looks like the under-ventilated flame, such as Fig. 5a, or the flame shape changes from the over-ventilated flame to the under-ventilated flame as shown in Figs. 4a, b, and 6a. The magnitude of the co-flow velocity can vary the fuel velocity that changes the flame shape from the over-ventilated to the under-ventilated flame at the second region. The stabilized point of these under-ventilated flames goes to the fuel nozzle as the fuel velocity increases, as shown in Figs. 4, 5a, and 6a. The flame is also highly oscillated in this region.

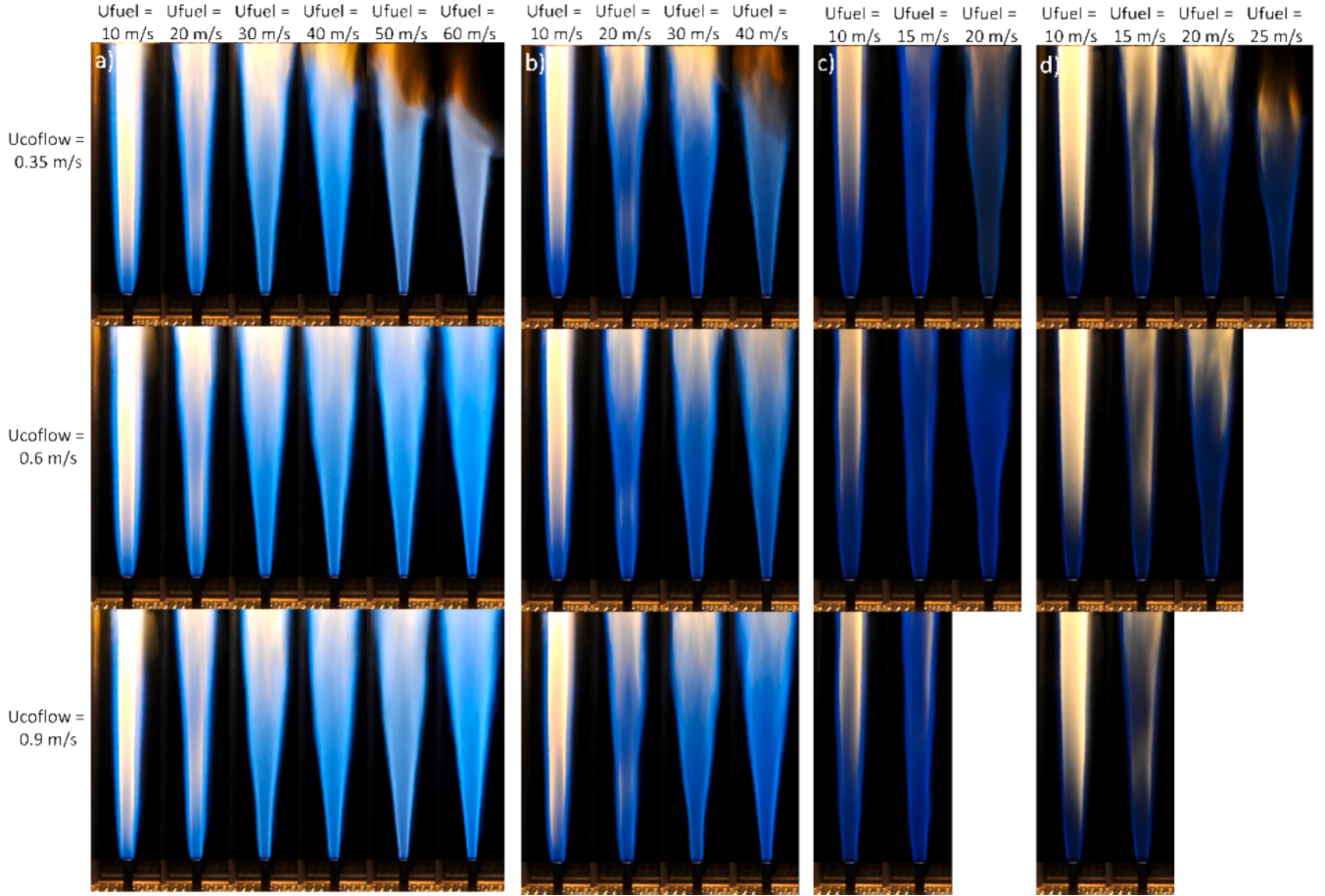
At the fourth region described in Figs. 5b, c, 6b, and c, the flame is lifted stably, and the flame stabilized point goes to the wall at the high fuel velocity. So, the flame anchoring mechanism can vary depending on the flame shape.

The main difference between the second and the fourth region is whether the under-ventilated flame happens or not. If the flame changes to the under-ventilated flame, such as the second region, the flammable range increases significantly. In contrast to this, if the flame cannot become the under-ventilated flame, the flame blows off relatively lower fuel velocity.

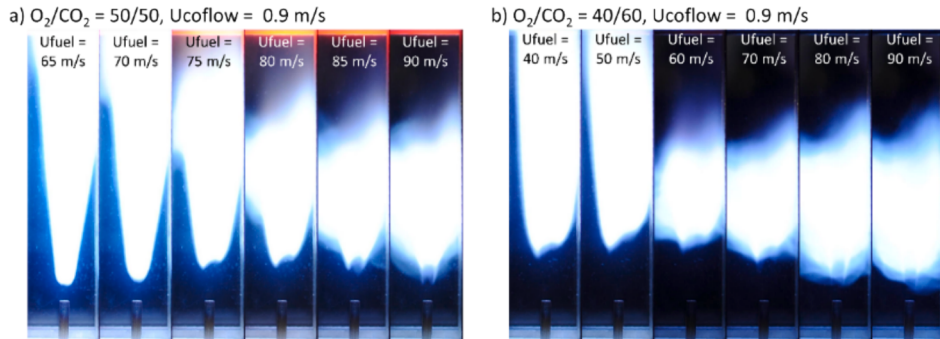
Blowoff behavior is also varied according to the flame shape. Under-ventilated flame in the first and second regions is extinguished near the nozzle. Over-ventilated flame in the fourth region is gone towards the top of the burner. Under-ventilated flame can be blown off due to the high fuel and air ratio. High flow velocity makes the over-ventilated flame blow off.

Fig. 7 shows the global equivalence ratio of lift-off, blowout, and blowoff conditions. The global equivalence ratio is calculated by considering the total mass flow of the fuel and the oxidizer. In the case of 50%/50% and 40%/60% of the O<sub>2</sub>/CO<sub>2</sub> mixture co-flow, the flame belongs to the second region except for low co-flow velocities in the first region, and there is no significant difference in the lift-off fuel jet velocity, although the co-flow velocity increases. So, the global equivalence ratio is inversely proportional to the co-flow velocity.

With 32%/68% of the O<sub>2</sub>/CO<sub>2</sub> mixture or the air co-flow, the lift-off conditions belong to the high global equivalence ratio range at the lower part of the second region. The flame can change to the under-ventilated



**Fig. 3.** DSLR images of attached flames (1/100 sec exposure time) with (a)  $O_2/CO_2 = 50/50$ , (b)  $O_2/CO_2 = 40/60$ , (c)  $O_2/CO_2 = 32/68$  and (d) air co-flow.



**Fig. 4.** DSLR flame images at 0.9 m/s of the co-flow velocity with (a)  $O_2/CO_2 = 50/50$  and (b)  $O_2/CO_2 = 40/60$ .

flame before the liftoff. So, the liftoff flame looks like the under-ventilated flame at the liftoff condition, as shown in Fig. 5a.

When the flame lifts off at the higher part of the second region near the fourth region, the liftoff flame looks like the over-ventilated flame in Fig. 6a, similar to the flame belonging to the fourth region in Fig. 6b. If the liftoff flame stability is so high, the flame can be sustained until a high equivalence ratio makes the under-ventilated flame. In this case, the under-ventilated flame increases the flammable range. However, if the flame stability gets weaker as the co-flow velocity increases, the liftoff over-ventilated flame cannot change to the under-ventilated flame and blows off. This is why the flame with 50 %/50 % and 40 %/60 % of  $O_2/CO_2$  mixture co-flow belongs to the second region at every flow condition. Higher stability can make the stable flame until the flame changes to the under-ventilated flame regardless of the high co-flow

velocity, as shown in Fig. 4.

The flame in the second region sometimes blows off without anchoring somewhere because the anchoring mechanism of the lifted under-ventilated flame is unstable. It can be shown that the flame can be anchored randomly in the third region despite the same flow condition. This unstable anchoring mechanism of the liftoff under-ventilated flame is also related to the highly oscillated flame in the second region.

The blowoff equivalence ratio of the second and third region is much higher than the upper flammable limit of the premixed flame ( $CH_4$ -air flame is 1.68 [37],  $CH_4$ -32 %  $O_2$ -68 %  $CO_2$  flame is 2.02,  $CH_4$ -40 %  $O_2$ -60 %  $CO_2$  flame is 2.19, and  $CH_4$ -50 %  $O_2$ -50 %  $CO_2$  flame is 2.35 [12]). Most  $CH_4$  may not participate in the reaction.

The flame blows off near the stoichiometric condition at the fourth region. The liftoff height of the flame in this region is sufficiently high to

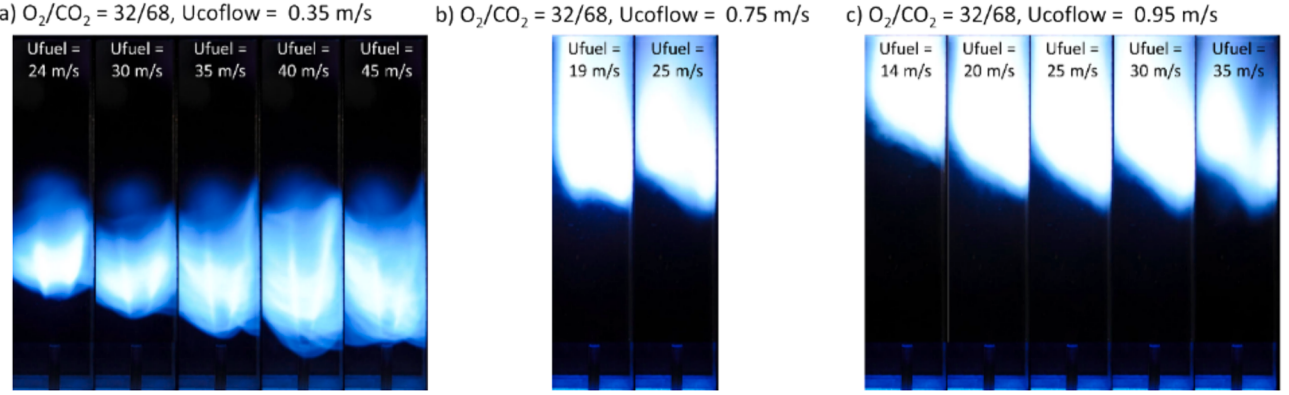


Fig. 5. DSLR flame images with  $O_2/CO_2 = 32/68$  at (a)  $0.35\text{ m/s}$ , (b)  $0.75\text{ m/s}$  and (c)  $0.95\text{ m/s}$  of the co-flow velocity.

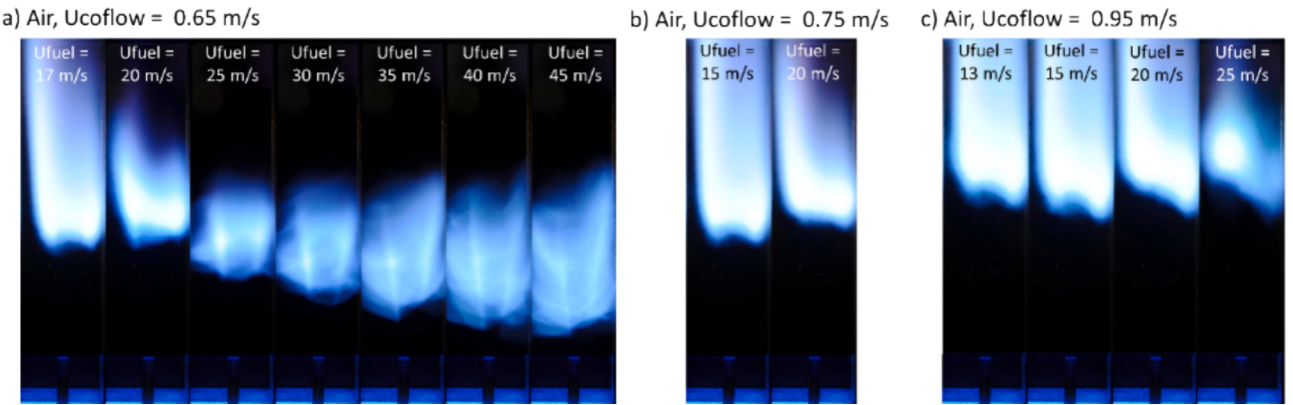


Fig. 6. DSLR flame images with the air co-flow at (a)  $0.65\text{ m/s}$ , (b)  $0.75\text{ m/s}$  and (c)  $0.95\text{ m/s}$  of the co-flow velocity.

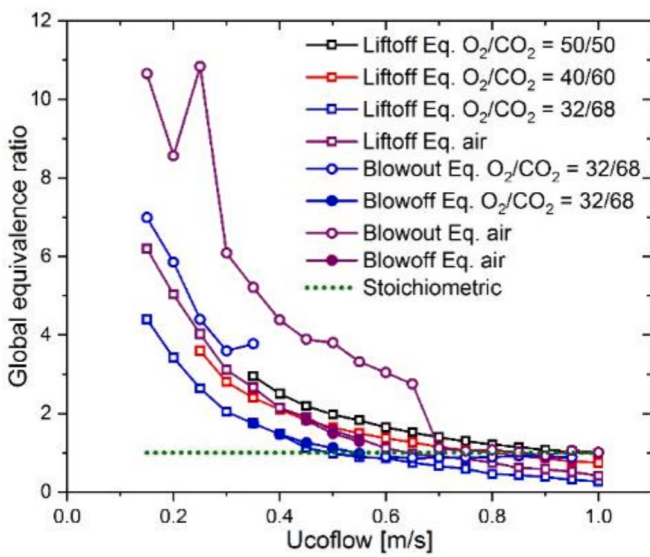


Fig. 7. Global equivalence ratio at the blowoff, blowout, and liftoff flow conditions.

mix each gas well. This high liftoff height can allow the liftoff flame to be considered as the partially premixed flame. The reactivity of flammable gas is the highest at the stoichiometric condition and decreases as increasing the co-flow velocity. So, the mixed gas can be burned up to the stoichiometric condition regardless of the co-flow velocity and the co-flow types.

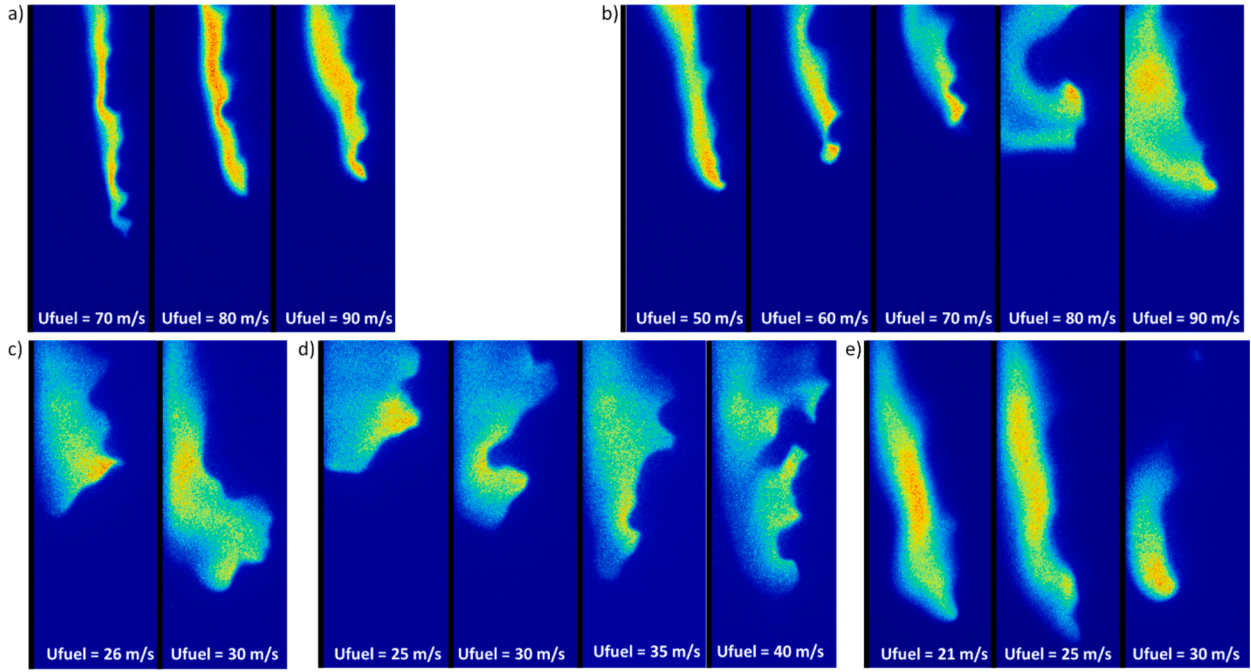
At the fourth region of flame stability, there are two types of flame anchoring mechanisms. One is the relation between the axial velocity of the flame base point and the turbulent flame speed. The other is the low-speed region near the wall due to the boundary layer. The liftoff flame is stabilized by balancing between the axial velocity and the turbulent flame speed at first. When the flame is about to blow out, the liftoff flame is anchored at the wall due to the low velocity of the boundary layer.

Fig. 8 shows half of the instantaneous OH-LIF images near flame base points of the liftoff flame.

OH layer thickness increase slightly at  $90\text{ m/s}$  of  $O_2/CO_2 = 50\% / 50\%$  % co-flow in Fig. 8a) and  $70\text{ m/s}$  of  $O_2/CO_2 = 40\% / 60\%$  % co-flow in Fig. 8b) although the under-ventilated flame occurs at  $75\text{ m/s}$  of  $O_2/CO_2 = 50\% / 50\%$  and  $60\text{ m/s}$  of  $O_2/CO_2 = 40\% / 60\%$  according to Fig. 4a) and b). As increasing the fuel velocity, the oscillation of the flame structure becomes larger. The OH layer becomes much thicker and moves to the wall at this condition. So, the flame base structure begins to be affected after the under-ventilated flame has progressed sufficiently.

In the case of  $O_2/CO_2 = 32\% / 68\%$  co-flow in Fig. 8c) and d), OH LIF signal is distributed widely, as similar to the OH structure with the high fuel velocity of  $O_2/CO_2 = 40\% / 60\%$  although the flame shapes in Figs. 4b and 5a) are different. As seen in Fig. 5b) and c), the liftoff height is relatively higher, and the flame sticks at the wall. High liftoff height can supply enough mixing length to make the premixed or partially premixed flames. The attached flame of  $O_2/CO_2 = 50\% / 50\%$  and  $40\% / 60\%$  contains the center red flame at  $20\text{ m/s}$  of the fuel velocity in Fig. 4a) and b). In contrast, the liftoff flames of  $O_2/CO_2 = 32\% / 68\%$  and air co-flow that have high liftoff height do not show the red flame region. And then, the flame is attached to the wall to find the low-velocity region. Highly mixing and attaching at the low-velocity region make widely distributed OH layer at  $O_2/CO_2 = 32\% / 68\%$  co-flow.

With the air co-flow, the OH layer is also thicker than that of the



**Fig. 8.** Instantaneous OH-LIF images near the flame base point, a)  $O_2/CO_2 = 50\% / 50\%$ , Uco-flow = 0.9 m/s, b)  $O_2/CO_2 = 40\% / 60\%$ , Uco-flow = 0.9 m/s, c)  $O_2/CO_2 = 32\% / 68\%$ , Uco-flow = 0.75 m/s, d)  $O_2/CO_2 = 32\% / 68\%$ , Uco-flow = 0.95 m/s, and e) air co-flow, Uco-flow = 0.65 m/s (black lines represent the wall).

higher  $O_2$  concentration co-flow because of the higher liftoff height. When the flame oscillates strongly while increasing the fuel velocity, as shown in Fig. 6a, the OH layer becomes shorter and distributes randomly.

Fig. 9 shows the liftoff height and the standard deviation of the lifted flame. The liftoff height is measured by DSLR images in Fig. 5, and the standard deviation is calculated by 100 images of OH PLIF results in Fig. 8. Once the flame structure changes from the over-ventilated flame to the under-ventilated flames (liftoff height decreases with the fuel jet velocity increase), the standard deviation increases significantly due to the flame oscillations. For example, if the flame shape is an under-ventilated flame, the standard deviation is about 1 mm at  $O_2/CO_2 = 50/50$  and 40/60, and 2 mm at the air co-flow. However, the standard deviation at  $O_2/CO_2 = 40/60$  becomes about 2 mm under the over-ventilated flames.

### 3.2. Liftoff height and critical velocity

The flame shape can be distinguished into over-ventilated flames and

under-ventilated flames. An under-ventilated flame is developed due to the small, confined burner geometry. So, the under-ventilated flame is not considered for scaling because this flame shape can be stabilized due to the boundary layer, and the unburned fuel can remain after the flame region. In terms of an over-ventilated flame, there are two possible sources: the balance between the flow velocity and the burning velocity, and the boundary layer. To compare the scaling result with references, the liftoff heights with the balancing mechanism should be selected. In this study, two criteria are used to filter it out. First, the flame liftoff height keeps increasing as jet velocity increases. Second, the flame location point should be located outside of the boundary layer. Considering that the co-flow is the laminar flow, the laminar boundary layer thickness can be calculated, and if the radial anchoring point of the lifted flame is located inside the boundary layer, the liftoff height with this condition is excluded for scaling.

Fig. 10 shows the liftoff height when the flame is the over-ventilated flame. At the second region where the flame changes from the over-ventilated to the under-ventilated flame, the flame is considered the over-ventilated flame until the liftoff height decreases continuously.

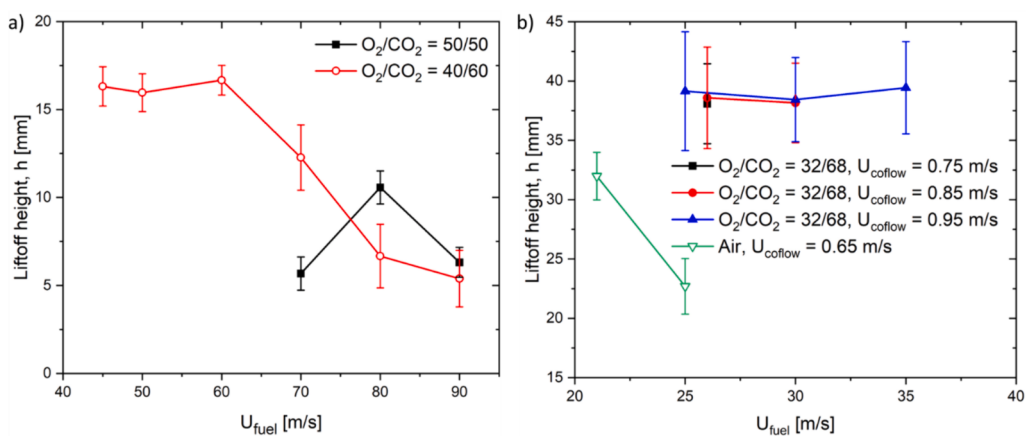


**Fig. 9.** Magnitude and the standard deviation of liftoff flames, (a)  $O_2/CO_2 = 40/60$  and 50/50, and (b)  $O_2/CO_2 = 32/68$ , and air co-flow.

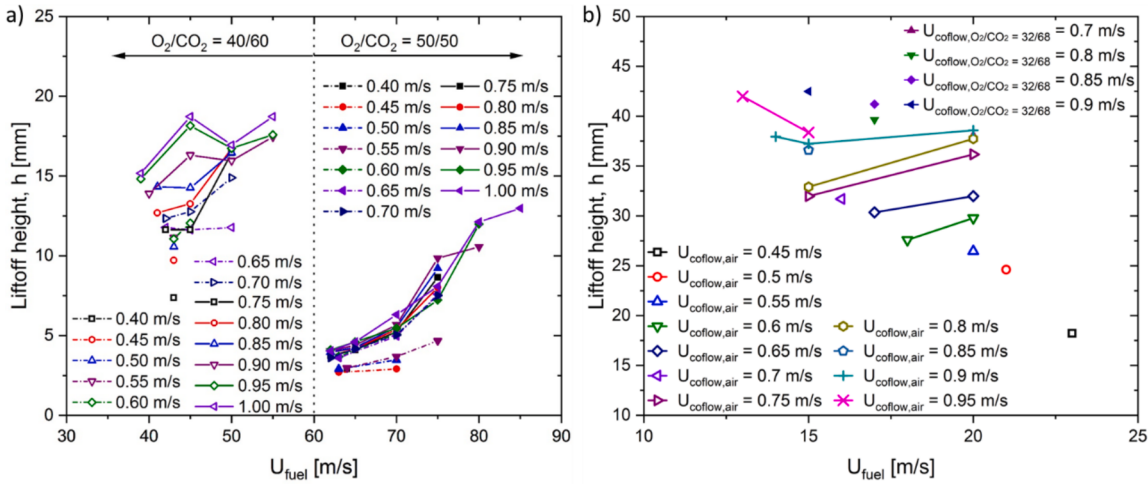


**Fig. 10.** Liftoff height of the over-ventilated flame, (a)  $O_2/CO_2 = 40/60$  and  $50/50$  and (b)  $O_2/CO_2 = 32/68$  and air co-flow.

This is because the liftoff height decreases as increasing the fuel velocity at the under-ventilated flame, such as Figs. 4a, b, and 6a.

The liftoff height increases with higher CO<sub>2</sub> concentration in the co-flow. The liftoff height of the air co-flow is similar to that of O<sub>2</sub>/CO<sub>2</sub> = 32/68. When the co-flow velocity is higher than 0.65 m/s, and the co-flow concentration is O<sub>2</sub>/CO<sub>2</sub> = 50/50, the liftoff increases significantly before the change to the under-ventilated flame. This rapid increase also happens at 0.75 m/s and 0.85 m/s of O<sub>2</sub>/CO<sub>2</sub> = 40/60 co-flow.

Fig. 11 shows the liftoff height as a function of the effective velocity suggested by Guiberti et al. [30]. Similar to the ref. [30],  $\beta$  and turbulent Schmidt number ( $Sc_t$ ) are adjusted to get a good collapse of the liftoff height with the highest R-square value. The number of  $\beta$  and  $Sc_t$  of O<sub>2</sub>/CO<sub>2</sub> = 50 %/50 % are much higher than those of other co-flow types. The value of  $\beta$  = 2.9 is a little higher but compatible with the common range of the CH<sub>4</sub>-air edge flame speed between 0 and 3S<sub>L</sub> [16,23–25]. It might be because the liftoff height at O<sub>2</sub>/CO<sub>2</sub> = 50 %/50 % is much lower than that of other papers. Liftoff height range is from 0 to 15 mm at O<sub>2</sub>/CO<sub>2</sub> = 50 %/50 %. In contrast, ranges of the liftoff height are 30 to 200 mm [16] and 30 to 90 mm [25]. But, the edge flame speed of CH<sub>4</sub>-air flame is from 0 to 25S<sub>L</sub> when the liftoff height is 30 mm [26]. The turbulent Schmidt number is also higher than that of other researches.

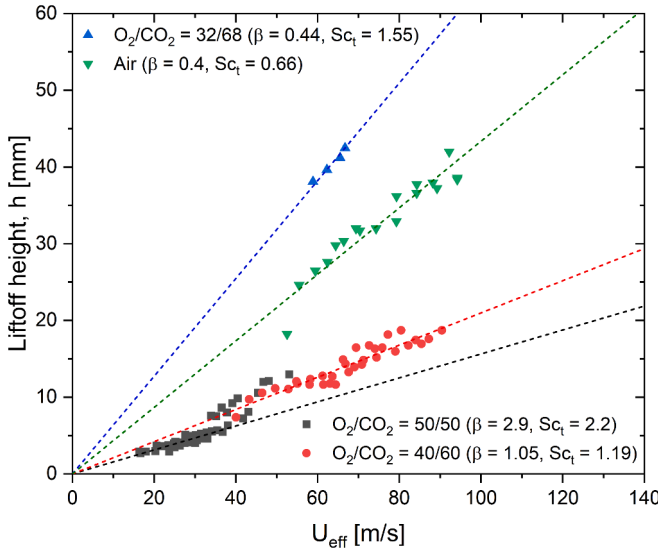


**Fig. 11.** Liftoff height as a function of the effective velocity for various co-flow types.

But, the turbulent Schmidt number can be higher than 2 depending on the environmental condition [38]. Therefore, values of  $\beta = 2.9$  and  $Sc_t = 2.2$  are reasonable numbers, although those are much higher than CH<sub>4</sub>-air liftoff flames.

In other co-flow types, values of  $\beta$  are much lower than in the O<sub>2</sub>/CO<sub>2</sub> = 50 %/50 % condition. It can be an effect of the wall and the higher flame length. At lower oxygen concentrations in the co-flow, the flame base point goes higher and moves to the wall to find the lower velocity region for stabilization. At the higher point, the fuel jet and the co-flow are well-mixed, so the velocity at the flame base point decreases. In addition, the flame base point becomes lower when it is close to the wall. Due to the wall effect, the velocity at the flame base in this experiment can be lower than other research values, as shown in Figs. 4, 5, and 8. The range of  $Sc_t$  from 0.34 to 1.06 is compatible with typical ranges of  $Sc_t$  from previous literature [38].

Fig. 12 shows the dimensionless liftoff height as a function of the dimensionless effective velocity, which is the same as Guiberti's suggestion [33]. In this reference,  $\beta = 1.5$  and  $Sc_t = 0.7$  are used to describe a good collapse on various fuels and elevated pressure conditions with air co-flow. With these values, dimensionless liftoff height with O<sub>2</sub> and CO<sub>2</sub> mixture co-flow shows a good collapsed relation at various O<sub>2</sub>/CO<sub>2</sub> concentrations. But this collapsed line does not pass through the origin (0,0) in Fig. 12a. According to the concept of the reference [33], averaged  $\beta$  and  $Sc_t$  of O<sub>2</sub>/CO<sub>2</sub> co-flows are considered to modify the slope and the y-intercept of Fig. 12a. The new collapsed line can pass through the origin, as shown in Fig. 12b. Nevertheless, there is still a big difference between dimensionless liftoff heights of air and O<sub>2</sub>/CO<sub>2</sub> mixture co-flows.

As increasing the effective velocity, some liftoff heights increase significantly from the linear trend of O<sub>2</sub>/CO<sub>2</sub> = 50 %/50 %. These points are also shown in Figs. 10 and 11. In Fig. 10a), the liftoff height of O<sub>2</sub>/CO<sub>2</sub> = 50 %/50 % increases rapidly at specific fuel velocities with higher co-flow velocities. For example, there is a significant increase of the liftoff height when the fuel velocity increases from 70 to 80 m/s and the co-flow velocity is 0.9 m/s. The flame base structure also changes from the convex shape to the concave shape at this point, as shown in Fig. 4a. This structure change further increases the liftoff height in addition to the effect of the fuel velocity. Also, two points are relatively higher than those at O<sub>2</sub>/CO<sub>2</sub> = 32 %/68 % and air co-flow. The liftoff flame anchors at a higher position when the flame lifts off at a higher co-flow velocity. After that, the flame descends downward.

In this paper, four additional parameters,  $\beta$ ,  $Sc_t$ , kinematic viscosity, and thermal diffusivity, are considered to modify the dimensionless liftoff height. When parameters change, the air result should not change significantly because it already shows a good relationship in the

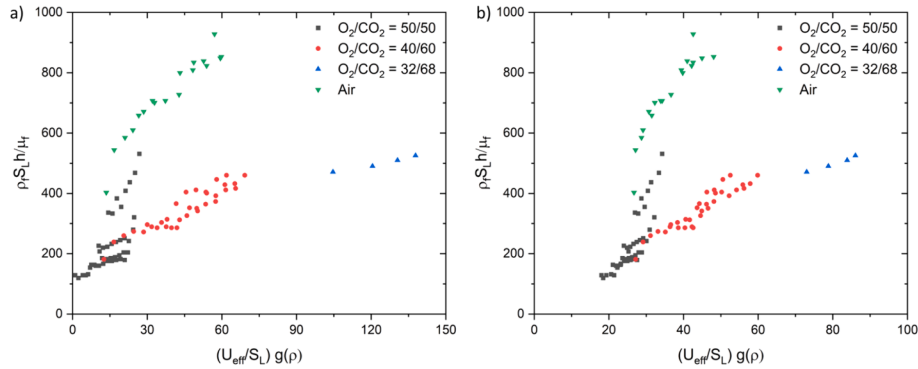


**Fig. 12.** Dimensionless liftoff height suggested by Guiberti et al. [33] as a function of the dimensionless effective velocity for various co-flow types by using (a)  $\beta = 1.5$ ,  $Sct = 0.7$ , (b)  $\beta = 1.2$ ,  $Sct = 1.4$ .

previous study.

In the previous study, the kinematic viscosity of the fuel is used to calculate dimensionless liftoff height. In contrast to this, stoichiometric mixture kinematic viscosity [39] is considered because the liftoff flame has the liftoff height as a pre-mixing length. There is no significant change in the kinematic viscosity between the  $CH_4$  ( $\nu_{CH_4} = 17.29 \times 10^{-6}$ ) and  $CH_4$ -air stoichiometric mixture ( $\nu_{CH_4\text{-air}} = 16.20 \times 10^{-6}$ ).

Thermal diffusivity can be used to calculate the dimensionless liftoff height [40]. The ratio of thermal diffusivity of stoichiometric flow between co-flow and air ( $\alpha_{\text{co-flow}}, \varphi=1/\alpha_{\text{air}}, \varphi=1$ ) is used to remain the air result as constant.

Fig. 13 shows the modified dimensionless liftoff height as a function of the dimensionless effective velocity. With the mixture viscosity and the thermal diffusivity ratio, Fig. 13a) shows a good collapse with every co-flow data except for several points under  $O_2/CO_2 = 50/50$ , as shown in Fig. 13a). It can be an error at the transient region from the under-ventilated to the over-ventilated flame. For example, the liftoff height no longer increases as much as lower jet velocities when the jet velocity increases from 75 to 80 m/s under  $O_2/CO_2 = 50/50$  and co-flow velocity is 0.9 m/s as shown in Fig. 9a. In this condition, the flame changes from the over-ventilated to the under-ventilated flame in Fig. 4a. So, the flame shape changes affect the flame liftoff height. Kalghatgi suggested the linear relation between the dimensionless velocity and liftoff height with the coefficient as 50 [27], and Guiberti's model also confirms this coefficient [33]. But, the coefficient of 18 shows a good linear relation rather than 50. The liftoff height can be affected by the burner geometry,

especially the fuel tube thickness [33]. In this study, the very thin tube is used to supply the fuel line. It might be one of reasons of the lower coefficient. In summary, the empirical coefficient calculated from the other burner may not be applicable. However, the empirical coefficient can be used for various co-flow conditions, considering the modified dimensionless liftoff height in Fig. 12, if the burner geometry does not change.

Fig. 14 shows the dimensionless effective velocity at which the flame lifts off as a function of the Reynolds number ratio and the density parameter. The dimensionless number on the x-axis represents the parameter affecting the mixing between the fuel and the co-flow. The dimensionless number on the y-axis describes the parameter of the flame. With these two dimensionless numbers, critical liftoff flow conditions can be predicted depending on whether the co-flow type is air or  $O_2/CO_2$  mixture.

#### 4. Conclusion

This paper studied the effect of the co-flow on the stability and the liftoff behavior of the  $CO_2$  diluted oxy-methane flame experimentally. In this study, the effect of the wall cannot be neglected because the wall affects the flammable limit and the flame behavior. The wall effect causes the difference from the previous flame stability studies of the coaxial diffusion jet flame. The important results are summarized as follows:

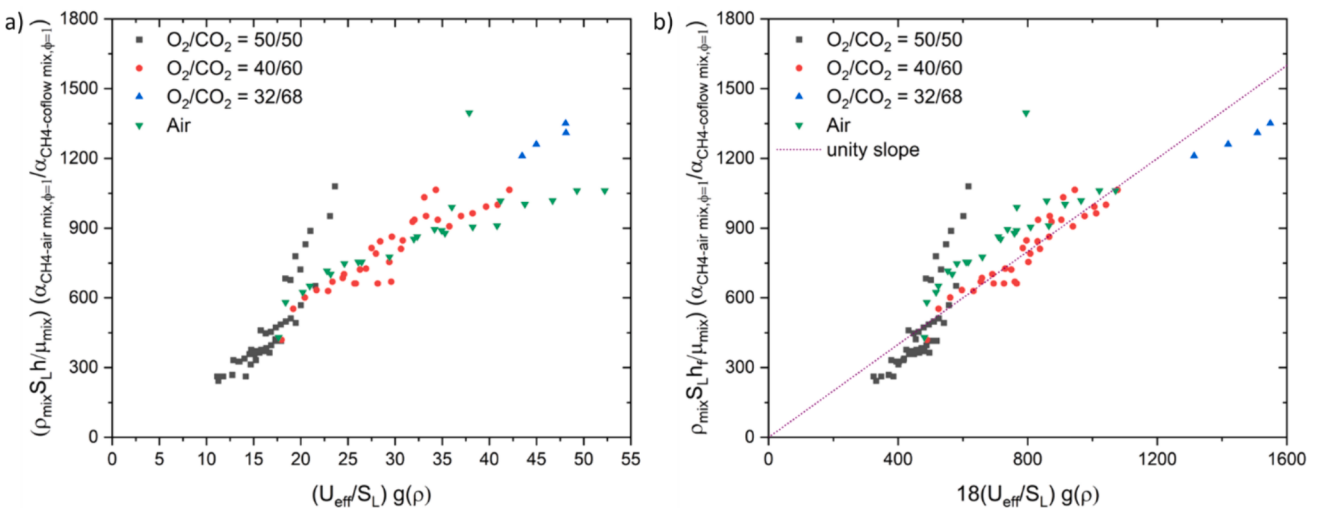


**Fig. 13.** Dimensionless liftoff height including the thermal diffusivity as a function of (a) the dimensionless effective velocity (b) with the coefficient to make the unity slope.

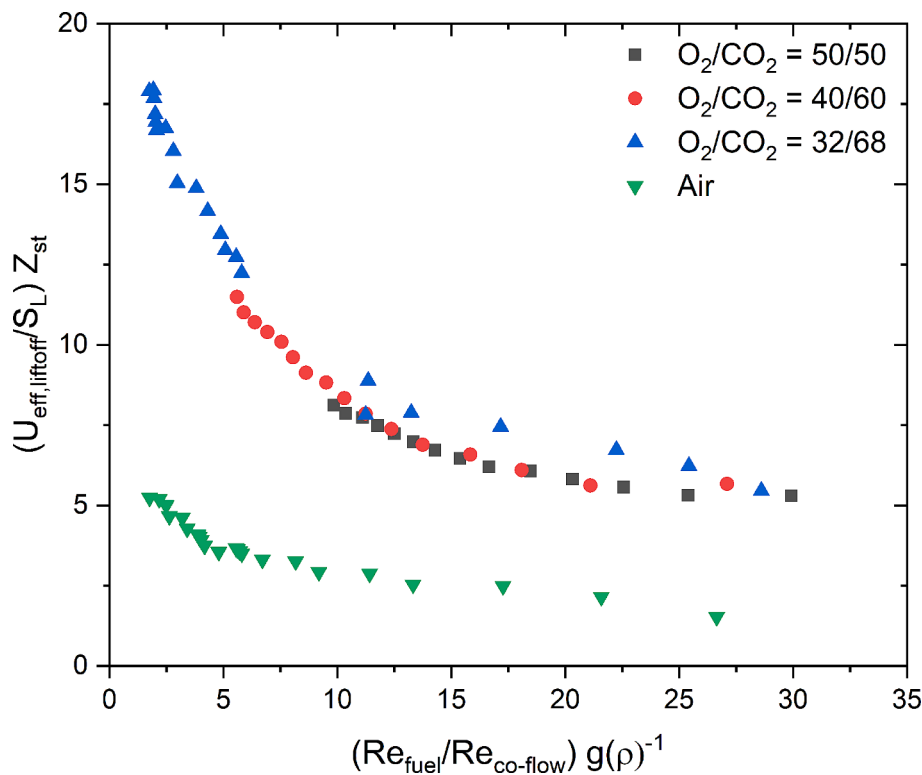


**Fig. 14.** Dimensionless effective velocity at critical liftoff conditions as a function of the Reynolds number and the density parameter.

- The under-ventilated flame can increase the flammable limit. Whether or not the flame shape changes to the under-ventilated flame depends on the stability of the liftoff flame. The lower the co-flow velocity and the higher oxygen concentration in the co-flow can make the higher stability. As decreasing the liftoff flame stability, the over-ventilated flame cannot change to the under-ventilated flame and blows out near the globally stoichiometric condition.
- By using the effective velocity proposed by Guiberti, the effective velocity at the liftoff condition shows a good collapse as a function of the co-flow velocity with various oxygen concentrations and air co-flow. The mixture kinematic viscosity and the thermal diffusivity ratio are included in Guiberti's model. Also, new coefficient  $\beta$  and turbulent Schmidt number are suggested for  $O_2/CO_2$  mixture co-flow. The modified effective velocity shows the possibility of the critical liftoff velocity prediction.

## Funding

The authors want to acknowledge that this work was funded by the clean combustion research center at King Abdullah University of Science and Technology (KAUST).

## CRediT authorship contribution statement

**Taesung Kim:** Writing – review & editing, Writing – original draft, Visualization, Methodology, Investigation, Formal analysis, Conceptualization. **Muhammad Bukar:** Visualization, Investigation. **Suman Basnet:** Visualization, Investigation. **Gaetano Magnotti:** Writing – review & editing, Validation, Supervision, Resources, Project administration, Funding acquisition.

## Declaration of competing interest

The authors declare that they have no known competing financial interests or personal relationships that could have appeared to influence

the work reported in this paper.

## Data availability

Data will be made available on request.

## References

- [1] Anderson RE, MacAdam S, Viteri F, Davies DO, Downs JP, Paluszewski A. Adapting gas turbines to zero emission oxy-fuel power plants. Volume 2: controls, diagnostics and instrumentation; cycle innovations; electric power, ASMEDC; 2008, p. 781–91. doi: 10.1115/GT2008-51377.
- [2] Cieutat D, Sanchez-Molinero I, Tsavas R, Recourt P, Aimard N, Précendé C. The Oxy-combustion burner development for the CO2 pilot at Lacq. Energy Procedia 2009;1:519–26. <https://doi.org/10.1016/j.egypro.2009.01.069>.
- [3] Allam R, Martin S, Forrest B, Fetsvedt J, Lu X, Freed D, et al. Demonstration of the Allam cycle: an update on the development status of a high efficiency supercritical carbon dioxide power process employing full carbon capture. Energy Procedia, vol. 114, Elsevier Ltd; 2017, p. 5948–66. doi: 10.1016/j.egypro.2017.03.1731.
- [4] Watanabe H, Shanbhogue SJ, Taamallah S, Chakraborty NW, Ghoniem AF. The structure of swirl-stabilized turbulent premixed CH4/air and CH4/O2/CO2 flames and mechanisms of intense burning of oxy-flames. Combust Flame 2016;174: 111–9. <https://doi.org/10.1016/j.combustflame.2016.09.015>.
- [5] Jourdainne P, Mirat C, Caudal J, Lo A, Schuller T. A comparison between the stabilization of premixed swirling CO2-diluted methane oxy-flames and methane/air flames. Fuel 2017;201:156–64. <https://doi.org/10.1016/j.fuel.2016.11.017>.
- [6] Zhao X, Shi B, Wang G, Gao W, Ma K, Li J. Stability limits of methane/oxygen mixtures diluted by N2 and CO2 under various oxygen contents. 2018 International Energy Conversion Engineering Conference, American Institute of Aeronautics and Astronautics Inc, AIAA; 2018. doi: 10.2514/6.2018-4802.
- [7] Kim HY, Lee J, Il KN. Effects of N2/CO2 dilution on flame propagation velocities and quenching distances of oxy-methane premixed mixtures using an Annular-Stepwise-Diverging-Tube (ASDT). Math Model Nat Phenom 2018;13. <https://doi.org/10.1051/mmnp/2018053>.
- [8] Kim TH, Park JW, Park HY, Park J, Park JH, Lim IG. Chemical and radiation effects on flame extinction and NOx formation in oxy-methane combustion diluted with CO2. Fuel 2016;177:235–43. <https://doi.org/10.1016/j.fuel.2016.03.012>.
- [9] Zhen H, Wei Z, Chen Z. Effect of N2 replacement by CO2 in coaxial-flow on the combustion and emission of a diffusion flame. Energies (Basel) 2018;11. <https://doi.org/10.3390/en11051032>.
- [10] Krishnamoorthy G, Ditaranto M. Predicting chemical flame lengths and lift-off heights in enclosed, oxy-methane diffusion flames at varying O2/CO2 oxidizer dilution ratios. J Power Technol 2017;97:370–7.

- [11] Khan AR, Anbusaravanan S, Kalathi L, Velamati R, Prathap C. Investigation of dilution effect with N<sub>2</sub>/CO<sub>2</sub> on laminar burning velocity of premixed methane/oxygen mixtures using freely expanding spherical flames. *Fuel* 2017;196:225–32. <https://doi.org/10.1016/j.fuel.2017.01.086>.
- [12] Hu X, Yu Q, Sun N, Qin Q. Experimental study of flammability limits of oxy-methane mixture and calculation based on thermal theory. *Int J Hydrogen Energy* 2014;39:9527–33. <https://doi.org/10.1016/j.ijhydene.2014.03.202>.
- [13] Halter F, Foucher F, Landry L, Mounaim-Rousselle C. Effect of dilution by nitrogen and/or carbon dioxide on methane and iso-octane air flames. *Combust Sci Technol* 2009;181:813–27. <https://doi.org/10.1080/00102200902864662>.
- [14] Hu X, Yu Q, Sun N, Liu J. Effects of high concentrations of CO<sub>2</sub> on the lower flammability limits of oxy-methane mixtures. *Energy Fuel* 2016;30:4346–52. <https://doi.org/10.1021/acs.energyfuels.6b00492>.
- [15] Chung SH, Lee BJ. On the characteristics of laminar lifted flames in a nonpremixed jet. vol. 86; 1991.
- [16] Muñiz L, Mungal MG. Instantaneous flame-stabilization velocities in lifted-jet diffusion flames. *Combust Flame* 1997;111:16–31. [https://doi.org/10.1016/S0010-2180\(97\)00096-5](https://doi.org/10.1016/S0010-2180(97)00096-5).
- [17] Wu CY, Chao YC, Cheng TS, Li YH, Lee KY, Yuan T. The blowout mechanism of turbulent jet diffusion flames. *Combust Flame* 2006;145:481–94. <https://doi.org/10.1016/j.combustflame.2006.01.004>.
- [18] Leung T, Wierzba I. The effect of co-flow stream velocity on turbulent non-premixed jet flame stability. *Proc Combust Inst* 2009;32 II:1671–8. <https://doi.org/10.1016/j.proci.2008.06.071>.
- [19] Takahashi F, Schmoll WJ. Lifting criteria of jet diffusion flames. *Symp (Int) Combust* 1991;23:677–83. [https://doi.org/10.1016/S0082-0784\(06\)80316-4](https://doi.org/10.1016/S0082-0784(06)80316-4).
- [20] Vanquickenborne L, van Tiggelen A. The stabilization mechanism of lifted diffusion flames. *Combust Flame* 1966;10:59–69. [https://doi.org/10.1016/0010-2180\(66\)90028-9](https://doi.org/10.1016/0010-2180(66)90028-9).
- [21] Tieszen S. A heuristic model of turbulent mixing applied to blowout of turbulent jet diffusion flames. *Combust Flame* 1996;106:442–62. [https://doi.org/10.1016/0010-2180\(96\)00008-9](https://doi.org/10.1016/0010-2180(96)00008-9).
- [22] Kaplan CR, Oran ES, Baek SW. Stabilization mechanism of lifted jet diffusion flames. *Symp (Int) Combust* 1994;25:1183–9. [https://doi.org/10.1016/S0082-0784\(06\)80757-5](https://doi.org/10.1016/S0082-0784(06)80757-5).
- [23] Han D, Mungal MG. Observations on the transition from flame liftoff to flame blowout. vol. 28; 2000.
- [24] Hasselbrink EF, Mungal MG. Characteristics of the velocity field near the instantaneous base of lifted non-premixed turbulent jet flames. *Symp (Int) Combust* 1998;27:867–73. [https://doi.org/10.1016/S0082-0784\(98\)80483-9](https://doi.org/10.1016/S0082-0784(98)80483-9).
- [25] Guiberti TF, Boyette WR, Roberts WL, Masri AR. Pressure effects and transition in the stabilization mechanism of turbulent lifted flames. *Proc Combust Inst* 2019;37: 2167–74. <https://doi.org/10.1016/j.proci.2018.08.033>.
- [26] Schefer RW, Namazian M, Filippoupolis EEJ, Kelly J. Temporal evolution of turbulence/chemistry interactions in lifted, turbulent-jet flames. *Symp (Int) Combust* 1994;25:1223–31. [https://doi.org/10.1016/S0082-0784\(06\)80762-9](https://doi.org/10.1016/S0082-0784(06)80762-9).
- [27] Kalghatgi GT. Lift-off heights and visible lengths of vertical turbulent jet diffusion flames in still air. *Combust Sci Technol* 1984;41:17–29. <https://doi.org/10.1080/00102208408923819>.
- [28] Upatnieks A, Driscoll JF, Rasmussen CC, Ceccio SL. Liftoff of turbulent jet flames - Assessment of edge flame and other concepts using cinema-PIV. *Combust Flame* 2004;138:259–72. <https://doi.org/10.1016/j.combustflame.2004.04.011>.
- [29] Montgomery CJ, Kaplan CR, Oran ES. The effect of coflow velocity on a lifted methane-air jet diffusion flame. 36th AIAA Aerospace Sciences Meeting and Exhibit, American Institute of Aeronautics and Astronautics Inc, AIAA; 1998. doi: 10.2514/6.1998-805.
- [30] Kumar S, Paul PJ, Mukunda HS. Prediction of flame liftoff height of diffusion/partially premixed jet flames and modeling of mild combustion burners. *Combust Sci Technol* 2007;179:2219–53. <https://doi.org/10.1080/00102200701407887>.
- [31] Moore NJ, Lyons KM. Leading-edge flame fluctuations in lifted turbulent flames. *Combust Sci Technol* 2010;182:777–93. <https://doi.org/10.1080/00102200903355017>.
- [32] Horn G, Thring MW. Angle of spread of free jets. *Nature* 1956;178:205–6. <https://doi.org/10.1038/178205a0>.
- [33] Guiberti TF, Boyette WR, Masri AR, Roberts WL. An experimental study of turbulent lifted flames at elevated pressures. *Combust Flame* 2019;203:301–12. <https://doi.org/10.1016/j.combustflame.2019.02.023>.
- [34] Han D, Mungal MG. Simultaneous measurements of velocity and CH distributions. Part 1: jet flames in co-flow. *Combust Flame* 2003;132:565–90. [https://doi.org/10.1016/S0010-2180\(02\)00515-1](https://doi.org/10.1016/S0010-2180(02)00515-1).
- [35] Smith G, Golden D, Frenklach M, Moriarty N, Eiteneer B, Goldenberg M, et al. GRI-Mech 3.0 n.d. [http://www.me.berkeley.edu/gri\\_mech/](http://www.me.berkeley.edu/gri_mech/) (accessed May 31, 2024).
- [36] Ghia KN, Lavan Z, Torda TP. Laminar mixing of heterogeneous axisymmetric coaxial confined jets. *AIAA J* 1969;7:2072–8. <https://doi.org/10.2514/3.5559>.
- [37] Cashdollar KL, Zlochower IA, Green GM, Thomas RA, Hertzberg M. Flammability of methane, propane, and hydrogen gases. vol. 13; 2000.
- [38] Gualtieri C, Angeloudis A, Bombardelli F, Jha S, Stoesser T. On the values for the turbulent schmidt number in environmental flows. *Fluids* 2017;2. <https://doi.org/10.3390/fluids2020017>.
- [39] Wilke CR. A viscosity equation for gas mixtures. *J Chem Phys* 1950;18:517–9. <https://doi.org/10.1063/1.1747673>.
- [40] Mason EA, Saxena SC. Approximate formula for the thermal conductivity of gas mixtures. *Phys Fluids* 1958;1:361–9. <https://doi.org/10.1063/1.1724352>.